SCIENTIFIC REPORTS
nature research

OPEN

Bio-assisted synthesized Pd nanoparticles supported on ionic liquid decorated magnetic halloysite: an efficient catalyst for degradation of dyes

Samahe Sadjadi[1*], Pourya Mohammadi[2] & Majid Heravi[2*]

Using natural materials, i.e. halloysite nanoclay that is a biocompatible naturally occurring clay and Heracleum persicum extract that can serve as a green reducing agent, a novel magnetic catalyst, Fe_3O_4/Hal-Mel-TEA(IL)-Pd, has been designed and fabricated. To prepare the catalyst, halloysite was first magnetized (magnetic particles with mean diameter of 13.06 ± 3.1 nm) and then surface functionalized with melamine, 1,4 dibromobutane and triethanolamine to provide ionic liquid on the halloysite surface (5 wt%). The latter was then used as a support to immobilize Pd nanoparticles that were reduced by Heracleum persicum extract. The characterization of the catalyst established that the loading of Pd in Fe_3O_4/Hal-Mel-TEA(IL)-Pd was very low (0.93 wt%) and its specific surface area was 63 m^2g^{-1}. Moreover, the catalyst showed magnetic property (Ms = 19.75 emu g^{-1}) and could be magnetically separated from the reaction. The catalytic performance of the magnetic catalyst for reductive degradation of methyl orange and rhodamine B in the presence of $NaBH_4$ in aqueous media was investigated. The activation energy, enthalpy, and entropy for the reduction of methyl orange were estimated as 42.02 kJ mol^{-1}, 39.40 kJ mol^{-1}, and −139.06 J mol^{-1} K^{-1}, respectively. These values for rhodamine B were calculated as 39.97 kJ mol^{-1}, 34.33 kJ mol^{-1}, and −155.18 J$mol^{-1}K^{-1}$, respectively. Notably, Fe_3O_4/Hal-Mel-TEA(IL)-Pd could be reused for eight reaction runs with negligible loss of the catalytic activity (~3%) and Pd leaching (0.01 wt% of the initial loading).

Application of low-cost, biocompatible and available natural compounds for the catalytic purposes has attracted tremendous attention. In this regard, use of halloysite (Hal) that is a dioctahedral 1:1 clay of the kaolin group has received growing interest[1–3]. Apart from high thermal, chemical and mechanical stability, the cylindrical morphology and opposite chemical and electrical properties of inner and outer surfaces of Hal, make it distinguished from other clays and broaden its utility for many applications such as cleaning[4], adsorbents[5,6], energy storage, catalysis, flame retardancy[1], sustainable release of drugs etc. Regarding catalysis, Hal not only can be utilized as a catalyst, but also can be applied as a support for the development of reusable catalysts. To date, various chemical, photochemical and electrochemical transformations such as coupling reactions[7,8], hydrogenation[9,10], oxidation have been promoted by using Hal-based catalysts[11–15]. Organic dyes such as methylene blue, rhodamine B (RhB) and methyl orange (MO) are toxic chemicals with potential health threat[16]. The release of these compounds in the industrial waste water has raised many concerns and motivated many studies for the efficient removal of these hazardous pollutants or their conversion into less toxic compounds[17,18]. In this context, several approaches, such as use of adsorbents, photodegradation, electrochemical degradations, membrane processes, oxidative processes and catalytic reduction of dyes have been developed[19–21]. Dye reduction is a catalytic decolorization process that is mostly promoted by metallic catalysts such as Pd, Pt and Au and a reducing agent such as $NaBH_4$[22].

[1]Faculty of Petrochemicals, Iran polymer and Petrochemicals Institute, 15 km Tehran-Karaj Highway, Pajuhesh Science and Technology Park, Pajuhesh Boulevard, postal cod; 14977-13115, PO Box 14975-112, Tehran, Iran. [2]Department of Chemistry, School of Science, Alzahra University, PO Box 1993891176, Vanak, Tehran, Iran. *email: s.sadjadi@ippi.ac.ir; m.heravi@alzahra.ac.ir

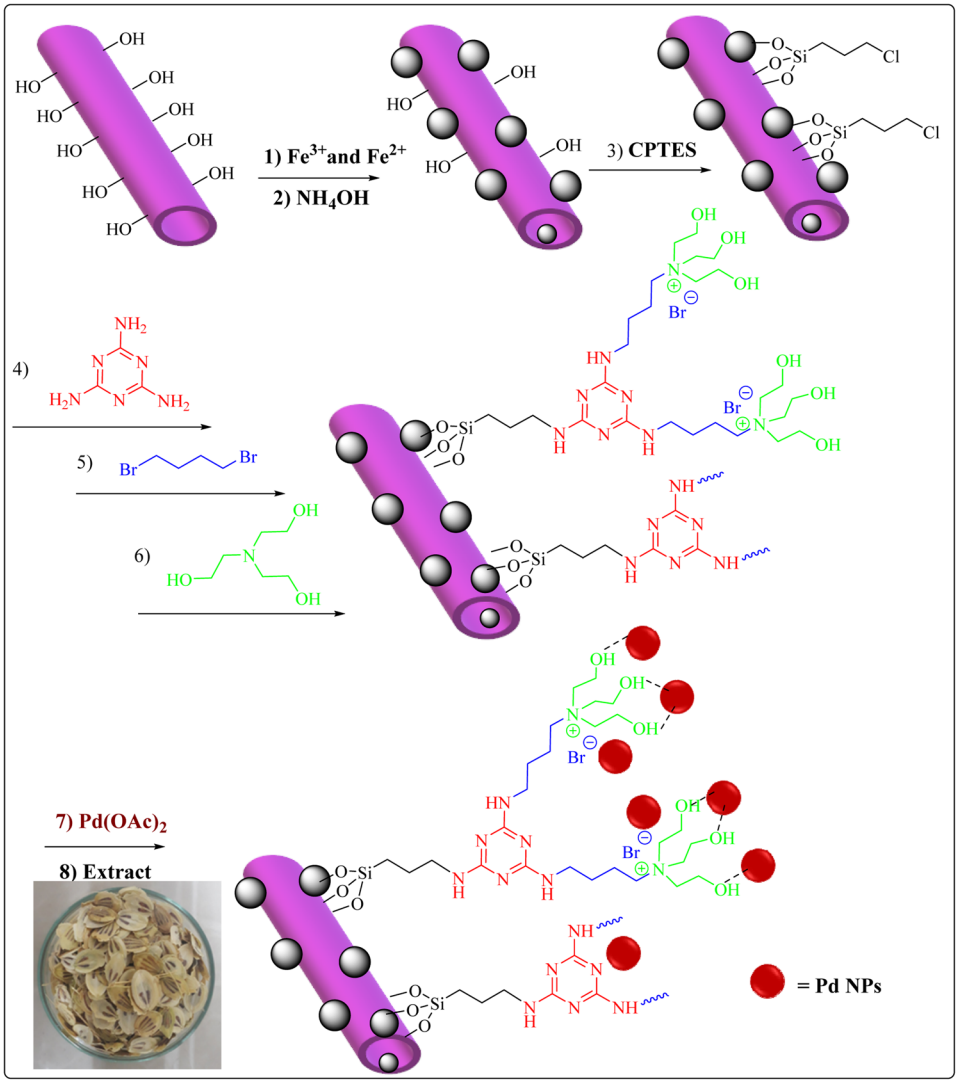

Figure 1. The schematic procedure for the synthesis of the catalyst.

In the continuation of our research on disclosing the catalytic utility of Hal[23,24], recently we have reported facile recovery and high reusability of magnetic Hal[25,26]. On the other hand, our research on the catalytic activity of IL-Hal hybrid[27,28] showed that the presence of ILs on the Hal can efficiently improve anchoring of nanoparticles and suppressing their leaching. In this work we design and synthesize a novel catalyst through multi-step procedure, Fig. 1, in which Hal was first magnetized and then reacted with melamine and 1, 4 di bromobutane. The resulting compound then tolerated reaction with triethanolamine to form IL. In the final step, Pd nanoparticles were supported on the IL-decorated magnetic Hal with the aid of Heracleum persicum extract as a biological reducing agent. To evaluate the catalytic activity of the resulting catalyst, the reduction of two dyes MO and RhB was studied in aqueous media. The reusability of the catalyst was also investigated. Moreover, the kinetic parameters, including activation energy, entropy and anthalpy of reduction of each dye have been calculated.

Results and discussions

Characterization. As depicted in Fig. 2, EDS analysis of the catalyst confirmed the presence of Al, Si and O atoms that can be attributed to the Hal structure. Notably, Si, O and C atoms can also represent the conjugation of CPTES. The presence of Fe atom indicated the successful magnetization of Hal. Observation of Pd atom also confirmed that Pd paricles were incorporated to the structure of the catalyst. The presence of C, N and Br atoms can be assigned to the organic moieties (melamine and IL). Figure S1 showed the elemental mapping analysis of Fe_3O_4/Hal-Mel-TEA(IL)-Pd. It was found that magnetic and Pd nanoparticles were well dispersed on the support.

In Fig. 3A the TEM image of Fe_3O_4/Hal is presented. As depicted, upon magnetization, Hal preserved its cylindrical morphology. Moreover, it can be seen that magnetic nanoparticles were located both on Hal exterior and interior surfaces. The measurement of the magnetic nanoparticle average size, Fig. 3A, showed that the synthetic procedure led to the formation of relatively small Fe_3O_4 nanoparticles (mean diameter of 13.06 nm with standard deviation of 3.1). The TEM analysis of the catalyst, Fig. 3B, also showed the cylinders of Hal, indicating

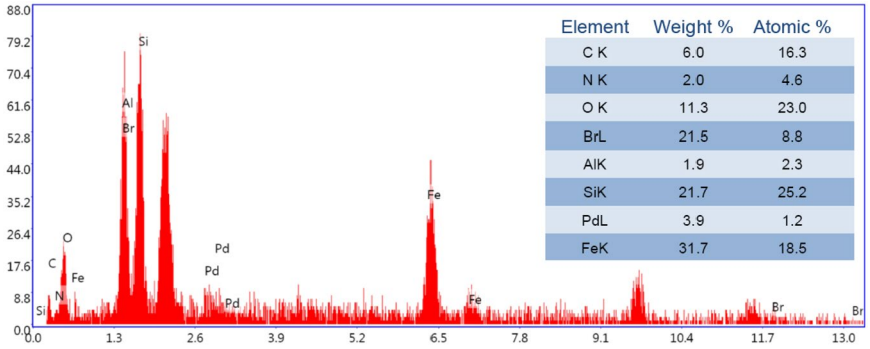

Figure 2. EDS analysis of the catalyst.

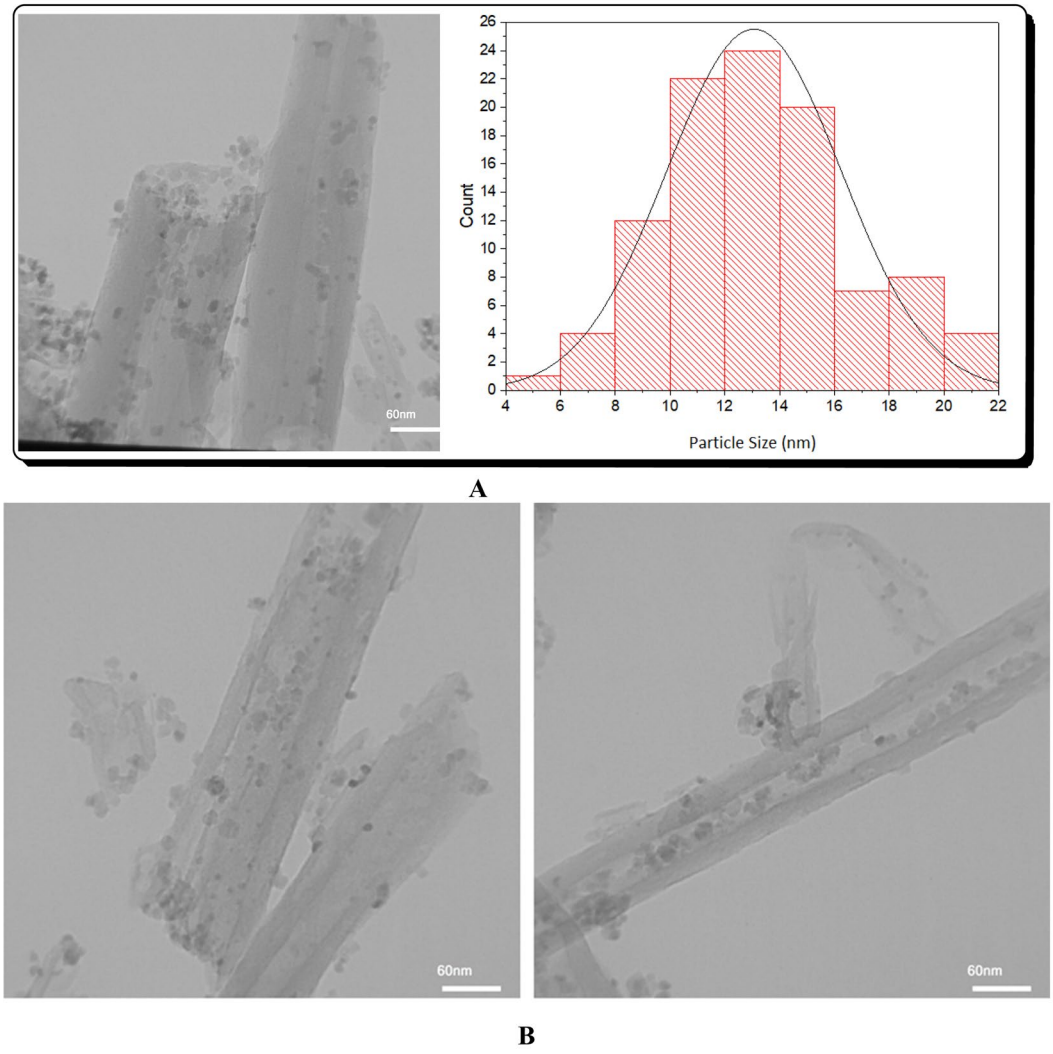

Figure 3. TEM image of Fe_3O_4/Hal (**A**) and TEM images of the catalyst (**B**).

that functionalization with organic moieties did not lead to the collapse of Hal structure. The dark black spots on the TEM image of the catalyst can be assigned to the magnetic and Pd nanoparticles.

In the next step, the structure of the catalyst was studied by recording its XRD pattern and comparing it with that of Fe_3O_4/Hal. As depicted in Fig. 4, the XRD pattern of Fe_3O_4/Hal showed two series of characteristic bands, i.e. the characteristic bands of Hal and those of magnetic nanoparticles. According to the literature, the characteristic bands of Fe_3O_4 can be observed at $2\theta = 30.52°$ (220), 35.5° (311), 43.18° (400), 57.22° (511), 62.73° (440) (denoted as F)[29]. The characteristic bands of Hal appeared at $2\theta = 12.4°$, 20.5°, 25.2°, 36.7°, 39.0°, 56.3° and 62.5°

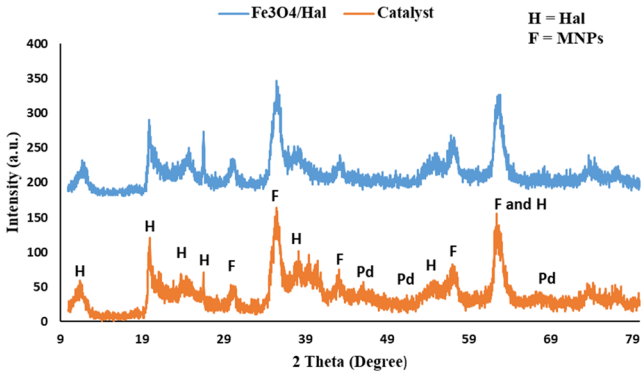

Figure 4. XRD patterns of the catalyst and magnetic Hal.

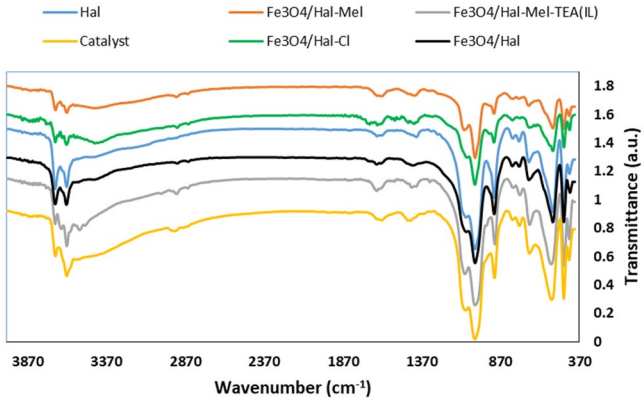

Figure 5. FTIR spectra of Hal, Fe_3O_4/Hal, Fe_3O_4/Hal-Cl, Fe_3O_4/Hal-Mel, Fe_3O_4/Hal-Mel-TEA(IL) and Fe_3O_4/Hal-Mel-TEA(IL)-Pd.

(the standard JCPDS card no. 29–1487, labeled as H)[30]. The XRD pattern of Fe_3O_4/Hal-Mel-TEA(IL)-Pd is very similar to that of Fe_3O_4/Hal and no displacement of the Hal and magnetic nanoparticles bands can be detected. This observation can indicate that decoration of magnetic Hal with melamine and IL as well as Pd incorporation did not affect the Hal structure and Hal maintained its tubular morphology. On the other hand, in the XRD pattern of Fe_3O_4/Hal-Mel-TEA(IL)-Pd some small additional bands at $2\theta = 40$ °, 51.6° and 68.4, JCPDS, Card No. 46–1043, labeled as Pd) can be observed that can be assigned to the Pd nanoparticles.

To study the magnetic feature of Fe_3O_4/Hal-Mel-TEA(IL)-Pd its magnetization curve was recorded and compared with that of bare magnetic nanoparticles, Fig. S2. The results showed that the magnetic saturation (Ms) value of Fe_3O_4/Hal-Mel-TEA(IL)-Pd (19.75 emu g^{-1}) was far lower than that of bare Fe_3O_4 (47.1 emu g^{-1}). It is worth noting that although the magnetic saturation of the catalyst was low, Fe_3O_4/Hal-Mel-TEA(IL)-Pd was magnetic enough to be readily separated from the reaction mixture by using an external magnet.

Next, the thermal stability of Fe_3O_4/Hal-Mel-TEA(IL)-Pd was studied by recording Fe_3O_4/Hal-Mel-TEA(IL)-Pd thermogram. Furthermore, to measure the content of IL and melamine, the thermograms of Hal and Fe_3O_4/Hal-Mel were also recorded and compared with that of Fe_3O_4/Hal-Mel-TEA(IL)-Pd, Fig. S3. Among three thermograms, Hal possessed the highest thermal stability and showed only two weight losses (loss of water below 200 °C and Hal dehydroxylation at about 470 °C). This is not beyond expectation, as bare Hal possesses no organic moieties. Followed by Hal, Fe_3O_4/Hal-Mel showed high thermal stability. In this sample, apart from the Hal weight losses, an additional weight loss at ~200 °C with weight loss of ~12 wt% is observed that can be attributed to the loss of silane and melamine functionalities. Comparing the thermogram of Fe_3O_4/Hal-Mel-TEA(IL)-Pd with that of Fe_3O_4/Hal-Mel, it was found that the content of IL was about 5 wt%.

In the following, the textural features (specific surface area and average pore size) of Fe_3O_4/Hal-Mel-TEA(IL)-Pd were investigated by using BET technique and compared with those of Hal, Fig. S4. It was found that the isotherms of both samples are of type II. The comparison of the specific surface area of the catalyst and Hal showed that the specific surface area of Fe_3O_4/Hal-Mel-TEA(IL)-Pd (63 m^2g^{-1}) was higher than that of bare Hal (48 m^2g^{-1}).

FTIR spectra of Hal, Fe_3O_4/Hal, Fe_3O_4/Hal-Cl, Fe_3O_4/Hal-Mel, Fe_3O_4/Hal-Mel-TEA(IL) and Fe_3O_4/Hal-Mel-TEA(IL)-Pd were recorded, Fig. 5. The characteristic bands that represent Hal included the bands at 1091 cm^{-1} (Si-O stretching), 3695 cm^{-1} and 3624 cm^{-1} (inner -OH functionalities) and 534 cm^{-1} (Al-O-Si vibration). The FTIR spectrum of Fe_3O_4/Hal showed the characteristic bands of Hal, implying the stability of Hal structure upon magnetization. Notably, the characteristic bands of Fe_3O_4 nanoparticles, i.e. the bands at 585 and 635 cm^{-1} (Fe-O stretching) overlapped with the bands of Hal. The FTIR spectrum of Fe_3O_4/Hal-Cl is very

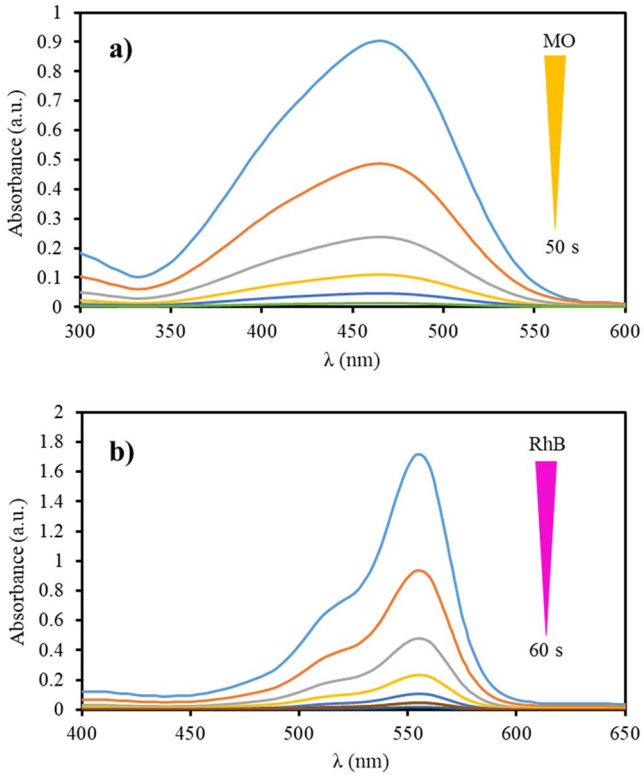

Figure 6. Reduction of MO (**a**) and RhB (**b**) dyes using Fe_3O_4/Hal-Mel-TEA(IL)-Pd in aqueous solution recorded by UV-vis spectroscopy.

similar to that of Fe_3O_4/Hal. In fact, the characteristic band of silane moiety (Si-O stretching) overlapped with that of Hal. The FTIR spectrum of Fe_3O_4/Hal-Mel exhibited the Hal characteristic bands, implying the fact that Hal structure is remained intact in the course of functionalization. Moreover, the band at 1648 cm^{-1} that can be representative of (-C = N) in the melamine structure overlapped with the Hal bands. The FTIR spectra of Fe_3O_4/Hal-Mel-TEA(IL) and Fe_3O_4/Hal-Mel-TEA(IL)-Pd were similar to that of Fe_3O_4/Hal-Mel. Similarly, the characteristic bans of IL overlapped with that of Fe_3O_4/Hal-Mel.

Finally, the zeta potential value of Fe_3O_4/Hal-Mel-TEA(IL)-Pd was measured and compared with that of Hal. Zeta potential value for pristine Hal was about −39.1 mV, while this value for Fe_3O_4/Hal-Mel-TEA(IL)-Pd was −32.4 mV. The reason for the lower zeta potential value of the catalyst can be attributed to the presence of positively charged ammonium salts on the surface of Hal.

Kinetic and thermodynamic studies. To evaluate the catalytic efficiency of the prepared catalyst, the reduction reaction of MO and RhB dyes was performed in the presence of $NaBH_4$ as a reducing agent and the progress of reaction was monitored using UV–visible spectroscopy. To elucidate the necessity of the use of Fe_3O_4/Hal-Mel-TEA(IL)-Pd, both dyes were treated with $NaBH_4$ for 24 h in the absence of the catalyst. The result confirmed that the reactions did not proceed without the catalyst, indicating the essential role of Fe_3O_4/Hal-Mel-TEA(IL)-Pd in the reduction process.

In the following, the effect of the amount of the catalyst on the reduction of MO and RhB was evaluated. To this purpose, reduction of dyes under similar condition in the presence of various amounts of Fe_3O_4/Hal-Mel-TEA(IL)-Pd (1, 2, 3, 4 and 5 mg) was carried out. The results, Table S1, showed that in the case of MO, the conversion of the reduction process increased with the increase of the catalyst loading from 1 to 2 mg. However, further increase of the catalyst amount had no effect on the reaction conversion. Regarding RhB, increase of the catalyst amount up to 4 mg led to the increase of the conversion of the reduction process, while further increase of this value to 5 mg did not result in any increase in the reaction conversion, Table S1. Considering these results the optimum catalyst amounts for MO and RhB were found to be 2 and 4 mg respectively.

The temporal UV–vis spectral changes of MO and RhB dyes in the course of the catalytic reduction in the presence of optimum amounts of the catalyst and $NaBH_4$ are illustrated in Fig. 6. The decrease of the absorbance at $\lambda_{max} = 465$ nm (MO) and $\lambda_{max} = 550$ nm (RhB) demonstrated efficient decolorization of dyes in a very short reaction time (50 s for MO and 60 s for RhB). To elucidate whether bare magnetic nanoparticles were catalytically active for the reduction of MO and RhB, the reduction reaction of both dyes in the presence of $NaBH_4$ was performed by using 4 mg bare magnetic nanoparticles as catalyst. Monitoring the progress of the reaction certified that within 1 min, MNPs did not promote the reduction of MO and RhB. This result confirmed that in 1 min that is the reaction time, in which the reduction reaction completed in the presence of Fe_3O_4/Hal-Mel-TEA(IL)-Pd, MNPs had no role in the reduction reaction, but facilitated the separation of the catalyst from the reaction media.

Dye	T (K)	k (min^{-1})	Ea (kJ/mol)	$\Delta S^{\#}$ (J/mol.K)	$\Delta H^{\#}$ (kJ/mol)
MO	298	0.045	42.02	−139.06	39.40
	303	0.050			
	308	0.067			
	313	0.101			
RhB	298	0.041	39.97	−155.18	34.33
	303	0.067			
	308	0.080			
	313	0.085			

Table 1. The thermodynamic and kinetic values of the reduction reaction of MO and RhB dyes in the presence of the Fe_3O_4/Hal-Mel-TEA(IL)-Pd catalyst.

Entry	Catalyst	k_{app} (min^{-1})	E_a (kJ/mol)	$\Delta S^{\#}$ (J/mol.K)	$\Delta H^{\#}$ (kJ/mol)	Ref.
1	CSIOAg[a]	$6*10^{-4}$ (s^{-1})	76.10	−29.20	73.60	32
2	IOAg[b]	NR	102.4	+41	99.9	32
3	CuO nanostructure (35 °C)	$1*10^{-2}$	59.84	−96.20	57.20	33
4	Co:La:$TiO_{2\ (30\ °C)}$	$7.72*10^{-3}$	NR	−69.15	35.33	34
5	$TiO_{2\ (30\ °C)}$	$5.26*10^{-3}$	NR	−69.76	24.07	34
6	**Fe_3O_4/Hal-Mel-TEA(IL)-Pd**	**$4.5*10^{-2}$ (s^{-1})**	**42.02**	**−139.06**	**39.40**	**This work**

Table 2. Comparison of the k_{app}, Ea, $\Delta S^{\#}$ and $\Delta H^{\#}$ values of previously reported catalysts for reduction of MO. a: Ag-coated chitosan-capped γ-Fe_2O_3 b: CSIOAg catalyst without chitosan NR: Not reported.

According to the literature, catalytic reduction of dye by metallic nanoparticles in the presence of excess amount of $NaBH_4$ is of pseudo-first-order kinetics[31]. The concentration of dye (C_t) in the course of the reduction can be calculated from the absorbance of the dye at its λ_{max}. Accordingly, the rate of the reduction reaction can be measured by considering the decrease of the absorbance of dyes at its λ_{max} versus time. As the ratio of the absorbance of dye at reduction time $t = A_t$ to initial time, $t = A_0$ is equal to the concentration ratio C_t/C_0, the apparent rate constant (k_{app}) can be defined by the following equations:

$$dC_t/dt = -k_{app}\, C_t \tag{1}$$

$$\ln C_t/C_0 = \ln A_t/A_0 = -k_{app} t \tag{2}$$

The values of k_{app} for the dyes can be calculated from the slope of ln (A_t/A_0) versus t (s) plot. The value of k_{app} obtained at various temperature (298, 303, 308 and 313 K) are reported in Table 1.

It was found that the kinetic energy of the reactants increased upon increasing of the reaction temperature. This observation can be attributed to the increase of the intensity of the collision of the reactants at elevated temperature. Based on Arrhenius equation (Eq. 3), the activation energies (E_a) of the reduction reactions of two dyes were estimated by plotting lnk vs. 1/T, Fig. S5 and Table 1. In those plots the R^2 value for MO and RhB were 0.935 and 0.864 respectively.

$$\ln k = \ln A - (E_a/RT) \tag{3}$$

In this equation E_a is activation energy, A stands for Arrhenius factor, T is temperature and R represents ideal gas constant = 8.314 JK^{-1} mol^{-1}. In the following, the thermodynamic parameters, i.e. the activation entropy ($\Delta S^{\#}$) and the activation enthalpy ($\Delta H^{\#}$) were calculated by using the Eyring equation (Eq. 4).

$$\ln(k/T) = \ln(k_B/h) + \Delta S^{\#}/R - \Delta H^{\#}/R(1/T) \tag{4}$$

In this equation, k_B (Boltzmann constant $=1.381 * 10^{-23}$ JK^{-1}) and h (the Planck constant $= 6.626 * 10^{-34}$ JK^{-1} mol^{-1}) are constant. Figure S6 shows the plots of ln(k/T) vs. 1/T for MO and RhB. In those plots the R^2 value for MO and RhB were 0.931 and 0.838 respectively. The entropy values of the reduction reaction of MO and RhB were calculated to be −139.06 and −155.18 $Jmol.K^{-1}$ respectively. Enthalpies of the reduction reactions were measured to be 39.40 and 34.33 $kJmol^{-1}$ for MO and RhB dyes, respectively (Table 1).

To confirm the merit of Fe_3O_4/Hal-Mel-TEA(IL)-Pd for the reduction of organic dyes, its performance for the reduction of MO was compared with some of the other catalysts that have been used for the reduction of this dye in the presence of $NaBH_4$, Table 2. The low value of k_{app} of Fe_3O_4/Hal-Mel-TEA(IL)-Pd compared to the tabulated catalysts showed that Fe_3O_4/Hal-Mel-TEA(IL)-Pd can catalyze the reduction of MO rapidly. Moreover, the low value of E_a for Fe_3O_4/Hal-Mel-TEA(IL)-Pd confirmed the efficiency of this catalyst. The comparison of $\Delta S^{\#}$ and $\Delta H^{\#}$ values of the catalyst with the reported ones also indicates that Fe_3O_4/Hal-Mel-TEA(IL)-Pd performance can be considered as an efficient catalyst for dye reductive degradation.

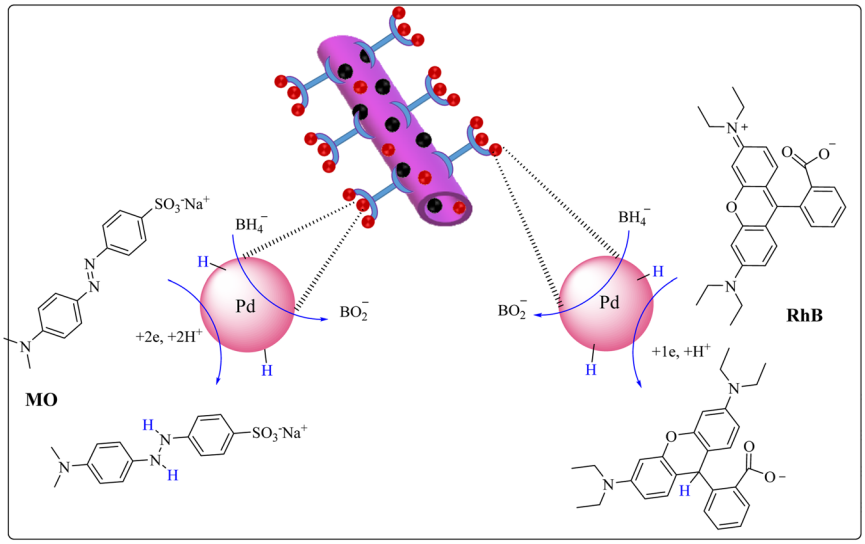

Figure 7. The plausible mechanism for the reduction of dye in the presence of Fe_3O_4/Hal-Mel-TEA(IL)-Pd.

The plausible mechanism for the reduction of MO and RhB in the presence of Fe_3O_4/Hal-Mel-TEA(IL) is presented in Fig. 7. As shown, sodium borohydride dissociates at the first step of the reaction to produce borohydride ions. Subsequently, BH_4^- ions are adsorbed on the surface of the Pd nanoparticles. Meanwhile, dyes are adsorbed onto the catalyst through π-π stacking interactions. Upon sorption of dyes on Fe_3O_4/Hal-Mel-TEA(IL)-Pd, the generated hydride ions transferred to them and dyes will be reduced. In the final step, the reduced dye will be detached from Fe_3O_4/Hal-Mel-TEA(IL)-Pd and allows the catalytic cycle to be repeated.

Reusability

The reusability of Fe_3O_4/Hal-Mel-TEA(IL)-Pd for the reduction of both MO and RhB was investigated. To this purpose, the catalyst was separated from the reaction mixture by using an external magnet and then reused for the next run of the reaction. This cycle was repeated for eight consecutive reaction runs and the obtained yields were measured and compared, Fig. 8. As shown in Fig. 8, Fe_3O_4/Hal-Mel-TEA(IL)-Pd exhibited excellent reusability and very slight loss of the catalytic activity after eight reaction runs was observed for both reactions. Encouraged by this result, the Pd leaching of the catalyst was investigated for the catalyst reused for eight reaction runs. Gratifyingly, Pd leaching was insignificant (0.01 wt% of the initial loading).

Next, the stability of Fe_3O_4/Hal-Mel-TEA(IL) upon reusing was investigated by recording its FTIR spectrum after eight reuse cycles for the reduction of MO and comparing it with that of fresh Fe_3O_4/Hal-Mel-TEA(IL)-Pd, Fig. S7. It was found that the spectrum of the reused Fe_3O_4/Hal-Mel-TEA(IL) was similar to that of the fresh one and no characteristic band of Fe_3O_4/Hal-Mel-TEA(IL)-Pd has been disappeared upon reusing.

Experimental

Preparation of magnetic Hal. In the first step of the preparation of the catalyst, Hal was magnetized. For this purpose, 2.5 g Hal was dispersed in 120 mL deionized water and the amounts of 1.37 g $FeCl_3$. $6H_2O$ and 0.5 g $FeCl_2$.$4H_2O$ were added to the Hal suspension. Then, the reaction mixture was stirred at 60 °C. In the following, 10 mL NH_3 was introduced to the reaction mixture. This mixture was then stirred vigorously for 1 h. At the end of the reaction, the precipitate was collected by an external magnet, washed several times with deionized water and dried at ambient temperature.

Functionalization of magnetic Hal with CPTES (Fe_3O_4/Hal-Cl). In the next step, magnetic Hal was functionalized with CPTES. More precisely, 1 g magnetic Hal was dispersed in 60 mL dried toluene and then 2.5 mL CPTES was added in a drop wise manner. Subsequently, the mixture was refluxed at 110 °C overnight. Upon completion of the reaction, the product was separated by an external magnet and washed with ethanol and dried at room temperature for 24 h.

Melamination of Fe_3O_4/Hal-Cl (Fe_3O_4/Hal-Mel). First, melamine (5 mmol) was dissolved in DMSO (100 mL). Subsequently, Fe_3O_4/Hal-Cl (1 g) was added to melamine solution and the resulting mixture was stirred vigorously and heated up to 100 °C for 24 h. Then, the product, Fe_3O_4/Hal-Mel, was collected by external magnet, washed with ethanol several times and dried at ambient temperature overnight.

Synthesis of Fe_3O_4/Hal-Mel-TEA(IL). At first, Fe_3O_4/Hal-Mel (1 g) was dispersed in CH_3CN by stirring. After that 1, 4 di bromobutane (10 mmol) was added to the aforementioned suspension and the resulting mixture was refluxed for 24 h. Then, the product (Fe_3O_4/Hal-Mel-Br) was separated by an external magnet and washed with ethanol and dried at room temperature overnight.

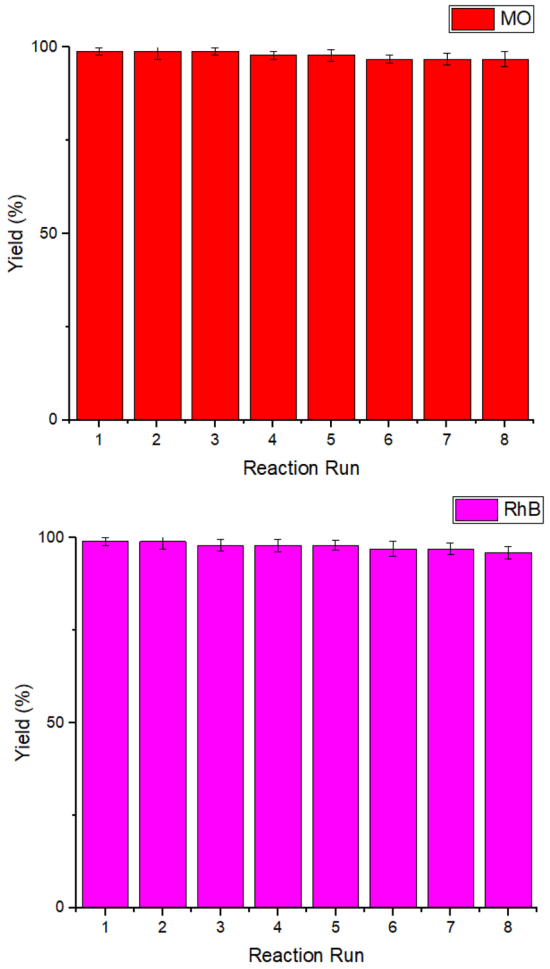

Figure 8. The results of the reusability of Fe_3O_4/Hal-Mel-TEA(IL)-Pd for the reduction of MO and RhB.

In the next step, 10 mmol of triethanolamine (TEA) was added dropwisely to the suspension of Fe_3O_4/Hal-Mel-Br in ethanol. The obtained mixture was then refluxed for 24 h. Finally, the product (Fe_3O_4/Hal-Mel-TEA(IL)) was separated by using an external magnet and washed with ethanol and dried at room temperature overnight.

Synthesis of Fe_3O_4/Hal-Mel-TEA(IL)-Pd NPs. To decorate Fe_3O_4/Hal-Mel-TEA(IL) with Pd nanoparticles, Fe_3O_4/Hal-Mel-TEA(IL) (1 g) was dispersed in deionized water (100 mL). Then, a solution of $Pd(OAc)_2$ (1.5 mM) was introduced and the resulting mixture was stirred vigorously at room temperature for 4 h. After that, 10 mL of Heracleum persicum extract was added and the mixture heated at 60 °C overnight. At the end of the reaction, the final product (Fe_3O_4/Hal-Mel-TEA(IL)-Pd NPs) was collected by an external magnet, washed with ethanol/water and dried at room temperature overnight. The schematic procedure for the synthesis of the catalyst is illustrated in Fig. 1. According to ICP result, the Pd content of Fe_3O_4/Hal-Mel-TEA(IL)-Pd was estimated as 0.93 wt%. Moreover, the content of magnetic nanoparticles was estimated to be 17.6 wt%.

Catalytic reduction of dye. To reduce the dyes, dye (2 mL) was dissolved in water and then proper amounts of Fe_3O_4/Hal-Mel-TEA(IL)-Pd and $NaBH_4$ solution (2 mL, 0.01 M) were added to the reaction mixture. The resulting mixture was subsequently stirred at different temperatures (25, 30, 35 and 40 °C). The progress of the degradation process was monitored by recording the time-dependent UV-vis absorption spectrum of the reaction mixture. At the end of the reaction, Fe_3O_4/Hal-Mel-TEA(IL)-Pd was collected magnetically, washed repeatedly with EtOH:H_2O (1:1) and dried.

Conclusion

Using Hal and Heracleum persicum extract as natural materials, Fe_3O_4/Hal-Mel-TEA(IL)-Pd was prepared through magnetization of Hal followed by surface functionalization and palladation. The composite was then applied as an efficient and magnetically separable catalyst for the reductive degradation of MO and RhB in aqueous media. The catalyst showed excellent catalytic activity for the reduction of both dyes in aqueous media. The activation energy, enthalpy, and entropy for the reduction of methyl orange were estimated as 42.02 kJ mol^{-1},

39.40 kJ mol^{-1}, and −139.06 J mol^{-1} K^{-1}, respectively. These values for RhB were calculated as 39.97 kJ mol^{-1}, 34.33 kJ mol^{-1}, and −155.18 J$mol^{-1}K^{-1}$, respectively. Fe_3O_4/Hal-Mel-TEA(IL)-Pd was also highly reusable and could be recovered magnetically and reused for eight reaction runs with only slight loss of its catalytic activity and Pd leaching.

Received: 11 February 2020; Accepted: 1 April 2020;
Published online: 16 April 2020

References

1. Li, Z., Liu, L., Jiménez González, A. & Wang, D.-Y. Bioinspired polydopamine-induced assembly of ultrafine $Fe(OH)_3$ nanoparticles on halloysite toward highly efficient fire retardancy of epoxy resin via an action of interfacial catalysis. *Polym. Chem.* **8**, 3926–3936, https://doi.org/10.1039/C7PY00660H (2017).
2. Yuan, P., Tan, D. & Annabi-Bergaya, F. Properties and applications of halloysite nanotubes: recent research advances and future prospects. *Appl. Clay Sci.* **112–113**, 75–93, https://doi.org/10.1016/j.clay.2015.05.001 (2015).
3. Lazzara, G. *et al.* An assembly of organic-inorganic composites using halloysite clay nanotubes. *Curr. Opin. Colloid Interface Sci.* **35**, 42–50, https://doi.org/10.1016/j.cocis.2018.01.002 (2018).
4. Cavallaro, G., Lazzara, G., Milioto, S. & Parisi, F. Halloysite Nanotubes for Cleaning, Consolidation and Protection. *Chem. Rec.* **18**, 1–11 (2018).
5. Anastopoulos, I. *et al.* A review on halloysite-based adsorbents to remove pollutants in water and wastewater. *J. Mol. Liq.* **269**, 855–868, https://doi.org/10.1016/j.molliq.2018.08.104 (2018).
6. Deng, L. *et al.* Effects of calcination and acid treatment on improving benzene adsorption performance of halloysite. *Appl. Clay Sci.* **181**, 105240, https://doi.org/10.1016/j.clay.2019.105240 (2019).
7. Hamdi, J., Blanco, A. A., Diehl, B., Wiley, J. B. & Trudell, M. L. Room-Temperature Aqueous Suzuki–Miyaura Cross-Coupling Reactions Catalyzed via a Recyclable Palladium@Halloysite Nanocomposite. *Org. Lett.* **21**, 3471–3475, https://doi.org/10.1021/acs.orglett.9b00042 (2019).
8. Sadjadi, S., Heravi, M. M., Masoumi, B. & Kazemi, S. S. Pd(0) nanoparticles immobilized on multinitrogen functionalized halloysite for promoting Sonogashira reaction: studying the role of the number of surface nitrogens in catalytic performance. *J. Coord. Chem.* **72**, 119–134, https://doi.org/10.1080/00958972.2018.1554214 (2019).
9. Vinokurov, V. *et al.* Core/Shell Ruthenium–Halloysite Nanocatalysts for Hydrogenation of Phenol. *Ind. Eng. Chem. Res.* **56**, 14043–14052, https://doi.org/10.1021/acs.iecr.7b03282 (2017).
10. Wenkai, D., Wenbo, W., Yuru, K. & Aiqin, W. Magnetic Halloysite/Fe_3O_4/AuNPs Nanocomposite as a Recyclable Efficient Catalyst for Hydrogenation of Congo Red and 4-Nitrophenol. *Curr. Environ. Eng.* **5**, 144–154, https://doi.org/10.2174/2212717804666171103110721 (2018).
11. Wang, R. *et al.* Photocatalytic Activity of Heterostructures Based on TiO_2 and Halloysite Nanotubes. *ACS Appl. Mater. Interfaces* **3**, 4154–4158, https://doi.org/10.1021/am201020q (2011).
12. Wang, H., Wu, D., Li, X. & Huo, P. Ce doping TiO_2/halloysite nanotubes photocatalyst for enhanced electrons transfer and photocatalytic degradation of Tetracycline. *J. Mater. Sci.: Mater. Electron* **30**, 19126–19136, https://doi.org/10.1007/s10854-019-02268-y (2019).
13. Mishra, G. & Mukhopadhyay, M. TiO_2 decorated functionalized halloysite nanotubes (TiO_2@HNTs) and photocatalytic PVC membranes synthesis, characterization and its application in water treatment. *Sci. Rep.* **9**, 4345, https://doi.org/10.1038/s41598-019-40775-4 (2019).
14. Vinokurov, V. A. *et al.* Halloysite Nanoclay Based CdS Formulations with High Catalytic Activity in Hydrogen Evolution Reaction under Visible Light Irradiation. *ACS Sustainable Chem. Eng.* **5**, 11316–11323, https://doi.org/10.1021/acssuschemeng.7b02272 (2017).
15. Li, X. *et al.* Halloysite–CeO_2–AgBr nanocomposite for solar light photodegradation of methyl orange. *Appl. Clay Sci.* **104**, 74–80, https://doi.org/10.1016/j.clay.2014.11.008 (2015).
16. Taghizadeh, A. & Rad-Moghadam, K. Green fabrication of Cu/pistachio shell nanocomposite using Pistacia Vera L. hull: An efficient catalyst for expedient reduction of 4-nitrophenol and organic dyes. *J. Clean. Prod.* **198**, 1105–1119, https://doi.org/10.1016/j.jclepro.2018.07.042 (2018).
17. Najafinejad, M. S., Mohammadi, P., Mehdi Afsahi, M. & Sheibani, H. Green synthesis of the Fe_3O_4@polythiophen-Ag magnetic nanocatalyst using grapefruit peel extract: Application of the catalyst for reduction of organic dyes in water. *J. Mol. Liqu.* **262**, 248–254, https://doi.org/10.1016/j.molliq.2018.04.052 (2018).
18. Naseem, K., Farooqi, Z. H., Begum, R. & Irfan, A. Removal of Congo red dye from aqueous medium by its catalytic reduction using sodium borohydride in the presence of various inorganic nano-catalysts: A review. *J. Clean. Prod.* **187**, 296–307, https://doi.org/10.1016/j.jclepro.2018.03.209 (2018).
19. Kurtan, U., Amir, M. & Baykal, A. Fe_3O_4@Nico-Ag magnetically recyclable nanocatalyst for azo dyes reduction. *Appl. Surf. Sci.* **363**, 66–73, https://doi.org/10.1016/j.apsusc.2015.11.214 (2016).
20. Ali, N. *et al.* Chitosan-coated cotton cloth supported copper nanoparticles for toxic dye reduction. *Int. J. Biol. Macromol.* **111**, 832–838, https://doi.org/10.1016/j.ijbiomac.2018.01.092 (2018).
21. Veerakumar, P., Panneer Muthuselvam, I., Thanasekaran, P. & Lin, K.-C. Low-cost palladium decorated on m-aminophenol-formaldehyde-derived porous carbon spheres for the enhanced catalytic reduction of organic dyes. *Inorg. Chem. Front.* **5**, 354–363, https://doi.org/10.1039/C7QI00553A (2018).
22. Adyani, S. H. & Soleimani, E. Green synthesis of Ag/Fe_3O_4/RGO nanocomposites by Punica Granatum peel extract: Catalytic activity for reduction of organic pollutants. *Int. J. Hydrog. Energy* **44**, 2711–2730, https://doi.org/10.1016/j.ijhydene.2018.12.012 (2019).
23. Bahri-Laleh, N., Sadjadi, S. & Poater, A. Pd immobilized on dendrimer decorated halloysite clay: Computational and experimental study on the effect of dendrimer generation, Pd valance and incorporation of terminal functionality on the catalytic activity. *J. Colloid Interface Sci.* **531**, 421–432, https://doi.org/10.1016/j.jcis.2018.07.039 (2018).
24. Sadjadi, S., Malmir, M., Lazzara, G., Cavallaro, G. & Heravi, M. M. Preparation of palladated porous nitrogen-doped carbon using halloysite as porogen: disclosing its utility as a hydrogenation catalyst. *Sci. Rep.* **10**, 2039, https://doi.org/10.1038/s41598-020-59003-5 (2020).
25. Sadjadi, S., Lazzara, G., Heravi, M. M. & Cavallaro, G. Pd supported on magnetic carbon coated halloysite as hydrogenation catalyst: Study of the contribution of carbon layer and magnetization to the catalytic activity. *Appl. Clay Sci.* **182**, 105299, https://doi.org/10.1016/j.clay.2019.105299 (2019).
26. Sadjadi, S., Malmir, M. & Heravi, M. M. A novel magnetic heterogeneous catalyst based on decoration of halloysite with ionic liquid-containing dendrimer. *Appl. Clay Sci.* **168**, 184–195, https://doi.org/10.1016/j.clay.2018.11.012 (2019).
27. Sadjadi, S. & Tavakolian, M. Halloysite - Poly (ionic liquid) Nanocomposite as an Efficient Catalyst Support: Study of the Effects of Ionic Liquid Nature and Content on the Catalytic Activity. *ChemistrySelect* **4**, 3369–3375, https://doi.org/10.1002/slct.201900493 (2019).

28. Sadjadi, S., Heravi, M. M., Malmir, M. & Masoumi, B. HPA decorated Halloysite Nanoclay: An efficient catalyst for the green synthesis of Spirooxindole derivatives. *Appl. Organomet. Chem.* **32**, e4113, https://doi.org/10.1002/aoc.4113 (2018).
29. Zhuang, L. *et al.* Preparation and characterization of Fe_3O_4 particles with novel nanosheets morphology and magnetochromatic property by a modified solvothermal method. *Sci. Rep.* **5**, https://doi.org/10.1038/srep09320 (2015).
30. He, Y., Xu, W., Tang, R., Zhang, C. & Yang, Q. pH-Responsive nanovalves based on encapsulated halloysite for the controlled release of a corrosion inhibitor in epoxy coating. *RSC Adv.* **5**, 90609–90620, https://doi.org/10.1039/C5RA19296J (2015).
31. Sahiner, N., Sagbas, S. & Aktas, N. Very fast catalytic reduction of 4-nitrophenol, methylene blue and eosin Y in natural waters using green chemistry: p(tannic acid)–Cu ionic liquid composites. *RSC Adv.* **5**, 18183–18195, https://doi.org/10.1039/C5RA00126A (2015).
32. Kaloti, M. & Kumar, A. Sustainable Catalytic Activity of Ag-Coated Chitosan-Capped γ-Fe_2O_3 Superparamagnetic Binary Nanohybrids (Ag-γ-Fe_2O_3@ CS) for the Reduction of Environmentally Hazardous Dyes -A Kinetic Study of the Operating Mechanism Analyzing Methyl Orange Reduction. *ACS omega* **3**, 1529–1545 (2018).
33. Deka, P., Hazarika, A., Deka, R. C. & Bharali, P. Influence of CuO morphology on the enhanced catalytic degradation of methylene blue and methyl orange. *RSC Adv.* **6**, 95292–95305 (2016).
34. Azad, K. & Gajanan, P. Photodegradation of methyl orange in aqueous solution by the visible light active Co: La: TiO_2 nanocomposite. *Chem. Sci. J.* **164** (2017).

Acknowledgements

The authors appreciate partial support of Iran Polymer and Petrochemical Institute and Alzahra University. M.M.H. is also thankful to IINSF for granted individual research chair.

Author contributions

Samahe Sadjadi: Funding acquisition, Methodology, Project administration, Supervision, Writing-original draft, Writing –review and editing. Pourya Mohammadi: Visualization, Writing original draft, Formal analysis Majid Heravi: Funding acquisition, Project administration.

Competing interests

The authors declare no competing interests.

Additional information

Supplementary information is available for this paper at https://doi.org/10.1038/s41598-020-63558-8.

Correspondence and requests for materials should be addressed to S.S. or M.H.

Reprints and permissions information is available at www.nature.com/reprints.

Publisher's note Springer Nature remains neutral with regard to jurisdictional claims in published maps and institutional affiliations.